

Magnetic and Electrical Properties of Electrodeposited Nickel Films

Musaab S. Sultan

Department of Networks and Information Security, Technical College of Informatics, University of Akre for Applied Sciences, 42004, Kurdistan Region, Iraq

Abstract—Magnetic and electrical properties of nickel (Ni) thin films produced by the electrodeposition technique under a range of growth times (30, 40, and 60 s) are investigated thoroughly using Magneto-Optical Kerr Effect (MOKE) magnetometry and Magneto-Resistance setup, respectively. To deeply understand these properties, the elemental composition, surface morphology, and bulk crystalline structure are analyzed using energy dispersive X-ray spectroscopy (EDS) with high-resolution scanning electron microscopy (HRSEM), grazing incidence X-ray reflectivity (GIXR), and X-ray diffraction measurements, respectively. EDS analysis confirms that these samples are free from impurities and contamination. An increase in coercive fields (~67 Oe) with wide distribution (58–85 Oe) across the film area and a slight variation in the shape of the loops are noticed by decreasing the film growth time (30 s). This is attributed to the deviations in the film surface morphology (defects), as confirmed by HRSEM and GIXR measurements. The angular dependence of the coercivity is nearly constant for each sample and most angles, indicating the similarity in the reversal behavior in such films. The sample resistance is found to be ~20.3 Ω and ~2.8 Ω for films with growth times of 40 s and 60 s, respectively. The coercivity of the AMR profiles and MOKE loops is consistent with each other, indicating that the magnetization at the surface performs similarly to that of their bulks. This article gives an indication that Ni films produced by this technique under such conditions are soft at longer deposition times and largely isotropic, which is more preferable in some magnetic applications.

Index Terms—Ferromagnetic Nickel films, Electrodeposition, Elemental composition, Magnetic and Electrical properties.

I. INTRODUCTION

Ferromagnetic thin films and nanostructures of cobalt, nickel (Ni), iron, and their alloys have been the topic of increasing interest for the past 40 years. This is due to their importance in scientific research and their significant demand in many industrial applications, such as giant magneto resistance (Elhoussine, et al., 2005; Karahan, Bakkalo and Bedir, 2007;

Thompson, 2008), magneto optical devices (Lee, et al., 2007; Sun, et al., 2005), and ultra-high density magnetic storage media in hard disk drives (Kunz, et al., 2010), as well as magnetic sensors (MS) (Kunz, et al., 2010; Sun, et al., 2005), and volatile magneto resistive random access memory (VMR-RAM) (Allwood, et al., 2005; Atkinson, Eastwood and Bogart, 2008; Kunz, et al., 2010; Lodder, 2004).

A variety of fabrication systems have been extensively used to produce these magnetic structures. These techniques include sputtering (Donald, 2003; Murakami and Birukawa, 2008; Uehara and Ikeda, 2003), thermal evaporation (Allwood, et al., 2005; Atkinson, Eastwood and Bogart, 2008; Donald, 2003), laser ablation (Donald, 2003), molecular beam epitaxy (Donald, 2003), electroless plating (Nazila and Georges, 2007), and electrodeposition (Peter, 2008; Possin, 1970; Sultan, 2013). Each method, however, has its own benefits and drawbacks. Among these systems, electrodeposition has been proven to be a simple, fast, and low-cost method. It also has benefits regarding reduced limitations on the shape and dimensions of the samples (Sun, et al., 2005).

The crystalline structure of such films has been extensively considered during the past few decades using different analytical techniques, which include transmission electron microscopy with selected area electron diffraction, and X-ray diffraction (XRD) analysis. These studies were carried out by changing the conditions or parameters under which they were produced. For instance, pH (Daimon and Kitakami, 1993; Fert and Piraux, 1999; Kafil, Fernando and Saibal, 2009; Lihu, et al., 2009; Nasirpouri, 2007; Possin, 1970; Rahman, et al., 2004; Ren, et al., 2009), temperature (Kafil, Fernando and Saibal, 2009; Nasirpouri, 2007), concentration of the electrolyte solution, growth voltage (Lihu, et al., 2009), deposition voltage mode (alternating current [AC] or direct current), annealing the samples at high temperatures (Guo, et al., 2003; Koohbor, et al., 2012; Qin, et al., 2002), and using a permanent magnet during the deposition process (Aravamudhan, et al., 2009; Coey and Hinds, 2001; Das, et al., 2008; Jin, et al., 2003; Sun and Chen, 2009; Tian, et al., 2005; 2008) are thoroughly discussed.

The magnetic properties of such ferromagnetic thin films were also investigated using a range of characterization systems, which include superconducting quantum interference device, vibrating sample magnetometry, torque



magnetometry, and alternating gradient magnetometry, as well as magnetic force microscopy. On the other hand, the Magneto-Optical Kerr Effect (MOKE) setup has also been used to demonstrate the magnetization behavior of a range of magnetic thin films (Azzawi, et al., 2016; Ganguly, et al., 2015; Michelini, et al., 2002), nanodots (Heyderman, et al., 2004), nanowires (Allwood, et al., 2003; Bryan, Atkinson and Allwood, 2006; Maruyama, et al., 1997), and more complex geometric shapes of nanostructures (Chen, et al., 2010; Das, et al., 2016; Eider, et al., 2016; Ester, et al., 2015; Lupu, Lostun and Chiriac, 2010; Philip, et al., 2016; Sharma, et al., 2009; Sultan, et al., 2012; Sultan, 2017a, 2017b; 2018; Vega, et al., 2012). However, in this setup, the reflected light is proportional to the amount of magnetization within the surface of the film, which depends on the polarization rotation of a polarized laser light following its reflection from a ferromagnetic sample to the skin depth (Allwood, et al., 2003). This is due to the absorption of the laser light in the medium, which is called the optical skin depth (Allwood, et al., 2003; Lupu, Lostun and Chiriac, 2010).

Magneto-Resistance (MR) setup is a powerful system adopted by many investigators to gain insight into the magnetic and electrical transport properties of ferromagnetic thin films (Alcer and Atkinson, 2017; Tokaç, et al., 2015), individual rectangular nanowires (Fernández-Pacheco, et al., 2008; Oliveira, et al., 2010; Oliveira, Rezende, and Azevedo, 2008 Tokaç, et al., 2015), rod nanowires embedded in their membranes (Fert and Piraux, 1999; Ferré, et al., 1997; Pignard, et al., 2000), and isolated rod wires (Rheem, 2007a; 2007b; 2007c; 2007d; Sultan, 2017) using the Anisotropic Magneto Resistance (AMR) effect. This is due to the sensitivity of AMR to the relative direction of the magnetic spins within the bulk of such materials with respect to the applied electrical current. Where the electrical resistance is at its highest value when the magnetic spins are parallel to the applied electrical current and at its lowest value when they are orthogonal to each other. This behavior is related to the anisotropic property of the electrons in the spin-orbit coupling, as investigated in further detail elsewhere (Cullity and Graham, 2009; Jiles, 1998).

Nevertheless, an understanding of the magnetic and electrical transport properties of electrodeposited

ferromagnetic thin films and nanostructures using surface and bulk characterization techniques such as MOKE and MR setup is crucial from a scientific and technological point of view. Therefore, in this article, ferromagnetic Ni thin films were prepared under different growth times using electrodeposition technique, and then their magneto- and electrotransport behavior was analyzed at room temperature using longitudinal MOKE magnetometry and MR setup, respectively. To deeply understand these properties, the chemical composition, surface structural variations (defects or imperfections), and bulk crystalline structure of such Ni films were thoroughly analyzed across the whole sample area.

II. EXPERIMENTAL DETAILS

Ferromagnetic Ni thin films with three different thicknesses were deposited onto Au/Cr/SiO₂/Si chips using the electrodeposition technique. The substrates (Si/SiO₂) were first thoroughly cleaned using acetone and isopropanol alcohol (IPA) and then dried with argon gas. The area of these substrates was approximately 2.4 × 22 mm². A gold (Au) film of 99.99% purity was placed onto these substrates with a thickness of ~10 nm on the SiO₂ side using thermal evaporation technique. To increase the adhesion of the gold film to the substrate, chromium (Cr) was deposited before the gold deposition of a thickness of ~3 nm. A schematic diagram of the gold-coated substrate (Au/Cr/SiO₂/Si) is shown in Fig. 1a.

These substrates were then used as cathodes (working electrodes) in the electrochemical cell, which is shown schematically in Fig. 1b with the gold-coated side facing toward the platinum counter electrode (anode) and electrically connected to the external circuit by a copper wire using silver paste. The reference electrode had a standard voltage of around 0.23 V and it was Ag/AgCl in saturated KCl solution.

To create Ni films, the chemical solution was ~0.57 M of NiSO₄, ~0.32 M of H₃BO₃, and the hydrogen ion concentration in the electrolyte solution was fixed at about 3.5–4. The voltage applied between the reference and counter electrodes was around -0.84 V. This voltage was selected

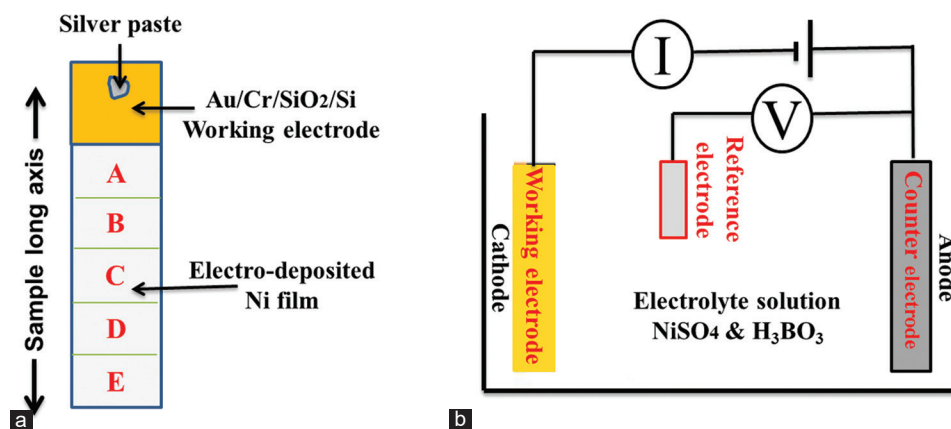


Fig. 1. (a) Gold-coated substrate (Au/Cr/SiO₂/Si) and (b) electrochemical cell with the gold-coated side (working electrode) facing toward the platinum counter electrode and electrically connected to the external circuit by a copper wire using silver paste.

according to a linear sweep voltammetry result. To prepare different thicknesses of Ni film, various deposition times of 30 s, 40 s, and 60 s were utilized. These growth times were chosen arbitrarily because most magnetic devices use ultra-thin ferromagnetic films. Once the electrodeposition was finished, the chips were washed thoroughly in distilled water, followed by IPA, and blown with argon gas. Further, information on the deposition procedure using this technique can be found in (Das, et al., 2008; Possin, 1970; Sultan, et al., 2012; Sultan, 2017a; 2017b; 2018).

Now, to analyze the elemental composition of these samples, energy-dispersive X-ray spectroscopy (EDS) analysis on the Hitachi-SU 70 was used. Whereas, to study the film roughness (surface morphology) and film thickness, high-resolution scanning electron microscopy (HRSEM) and grazing incidence X-ray reflectivity (GIXR) measurements were established, respectively. Finally, to measure the bulk crystalline structure of such thin films, the XRD system equipped in the Jordan Valley Bede diffractometer D1 was utilized. For more theoretical (Bowen and Tanner, 2006; Brundle, Evans and Wilson, 1992; Cullity and Stock, 2001; Cullity and Graham, 2009) and experimental (Bede REFS, 2007; Bowen and Mendis, 2012; Jordan Valley, 2007; 2008; Parratt, 1954; Wormington, et al., 1999) details on these analytical investigative techniques, please refer to the references (Bede REFS, 2007; Bowen and Tanner, 2006; 2012; Brundle, Evans and Wilson, 1992; Cullity and Stock, 2001; Cullity and Graham, 2009; Jordan Valley, 2007; 2008; Parratt, 1954; Wormington, et al., 1999).

The magnetic analyses were performed at room temperature using a highly sensitive longitudinal MOKE setup. In this technique, the laser light was focused onto the chip with a spot radius of around 2.5–3 μm . The change in the angle of reflected light (Kerr signal) is proportional to the longitudinal component of the magnetic state within the film surface plane.

All the chips were placed on a movable stage holder, which was located between the two poles of an AC electromagnet coil with a magnetic strength of ± 450 Oe, at an angle of $\sim 45^\circ$ with respect to the optical axis. To distinguish the real measurements from the background noise, all the MOKE measurements were done for repeated loops averaged over 3.5 min to satisfactorily reduce the noise and increase the reflected Kerr signal. The obtained hysteresis loops were the reflected Kerr light against the externally applied magnetic

field. More theoretical (Brundle, Evans and Wilson, 1992; Cullity and Graham, 2009; Jiles, 1998) and experimental (Eastwood, 2009; Lupu, Lostun and Chiriac, 2010; Sultan, et al., 2012; Sultan, 2017a; 2017b; 2018) details on the MOKE setup and its measurements can be found elsewhere.

The electrical and magnetic transport behavior of such films was also investigated using a room-temperature Magneto-Resistance setup, which is schematically shown in Fig. 2. This system was controlled by a digital computer using the LabVIEW program. The chips were placed on a rotation step between the pole pieces of an electromagnet with a maximum magnetic field of around ± 1 kOe and covered with an electrically and thermally shielded cover.

Fig. 3 shows a schematic diagram and a photograph of the sample holder of the four-point probe used in this research. It consisted of four equally spaced pieces of phosphor bronze plates (plated with gold) with a finite diameter. These tips were supported by springs on the other end to reduce film damage during the measurements. Further, details on the MR setup and its measurements can be found in (Armstrong, 2010; Brundle, Evans and Wilson, 1992; Cullity and Graham, 2009; Jiles, 1998; Sultan, 2017).

To perform the electrical measurements, the current was applied to the outer probes using a high-impedance current supply, whereas a voltmeter was connected to measure the voltage across the inner probes. The inner probe spacing was ~ 0.7 cm, whereas the outer probe spacing was ~ 1.2 cm, as schematically shown in Fig. 3. These measurements were performed using an electrical direct current of around 1 mA at room temperature. However, using higher electrical currents might increase the joule heating and destroy the sample.

The applied magnetic field was scanned between +1 kOe and -1 kOe. The chip carrier could be rotated at an angle between 0° and 90° with respect to the external magnetic field, allowing the investigations to be carried out at different angles. Once the current was applied to the sample, 50 measurements would be made and averaged to determine the electrical resistance. For each chip, the measurements were repeated four times to gain insight into the signal and noise background.

III. RESULTS AND DISCUSSION

The following subsections investigate the magneto- and electro-transport properties of electrodeposited Ni films

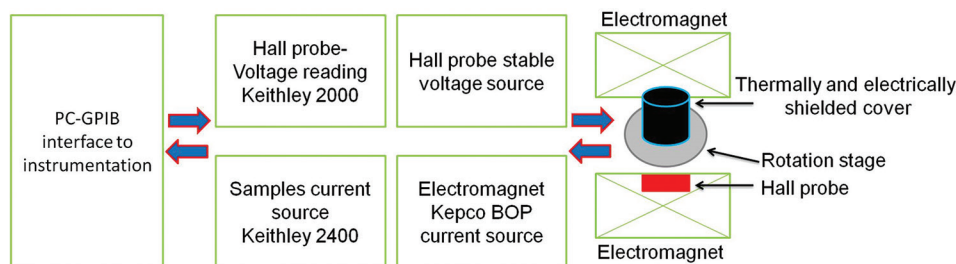


Fig. 2. A block diagram of the magneto resistance setup used in this article to discuss the electro- and magneto-transport properties of electrodeposited Ni thin films. Modified from (Armstrong, 2010).

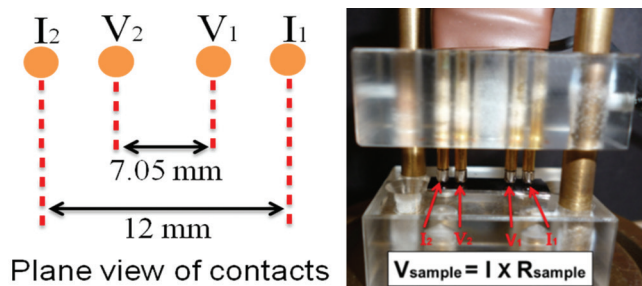


Fig. 3. A schematic diagram of the plane view of contacts for a four-point probe and a photograph of its sample holder. It consists of four equally gold-plated tips with a finite diameter.

prepared under different growth times using MOKE and MR setups, respectively, which are the main purpose of this study (Kacel, et al., 2018; Parlaka, et al., 2015; Rizwan, et al., 2021). To precisely analyze these properties, the chemical composition, surface morphology, thickness, and bulk crystalline structure of such thin films were firstly investigated using EDS with HRSEM, GIXR, and XRD measurements, respectively.

A. Elemental Composition, Surface, and Bulk Structure Analyses

To ascertain the elemental composition of such Ni films, all the samples were measured at different arbitrary locations (A, B, C, D, and E shown in Fig. 1a) using EDS analysis. These analyses were performed with support from (Bowen and Mendis, 2012). An example of the EDS measurement of Ni film prepared under a 40 s deposition time is shown in Fig. 4. The identification of the peaks is related to Ni, Au, O, and Si. The Au and Si contents reflect the elemental composition of the substrate.

A small amount of oxygen was noticed in most of the samples and might have been formed by oxidation during or after the electrodeposition. Significantly, these analyses confirm that these samples are free from impurities and contamination, which has been observed elsewhere (Das, et al., 2008).

Now, to investigate the surface morphology of such Ni samples, detailed of HRSEM imaging was undertaken. Micrographs example at three different locations on the surface of Ni film that was produced under 40 s deposition time is shown in Fig. 5. These measurements demonstrated that there were defects or imperfections of different sizes distributed randomly on these specimens. These defects were found to be more remarkable at lower film growth times. This is because decreasing the film growth time will decrease the film thickness which in turn increases the defects and non-uniformity. These imperfections are more likely to occur as a result of gas bubbles occurring during the electrodeposition process or might be due to the inhomogeneous density of the electrolyte solution throughout the electrochemical cell during the fabrication process. Thus, the Ni films prepared by this technique under such conditions are more likely to be non-uniform and have an irregular surface morphology. This result will be discussed in more detail in other research using other compositions of ferromagnetic thin films.

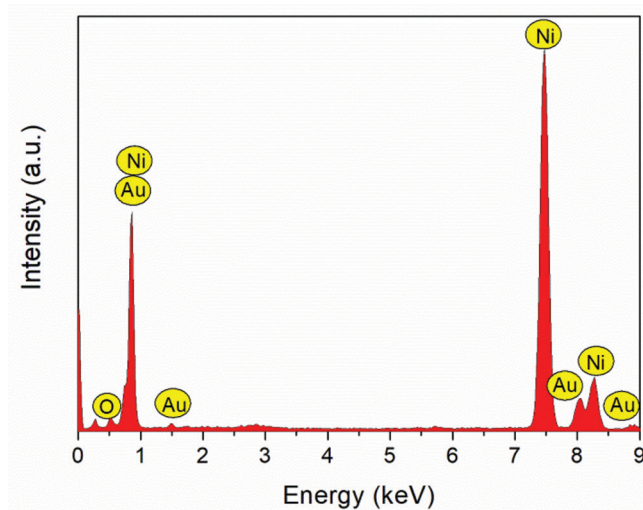


Fig. 4. An example of energy-dispersive X-ray spectroscopy measurement of nickel film prepared under a 60 s deposition time (Bowen and Mendis, 2012).

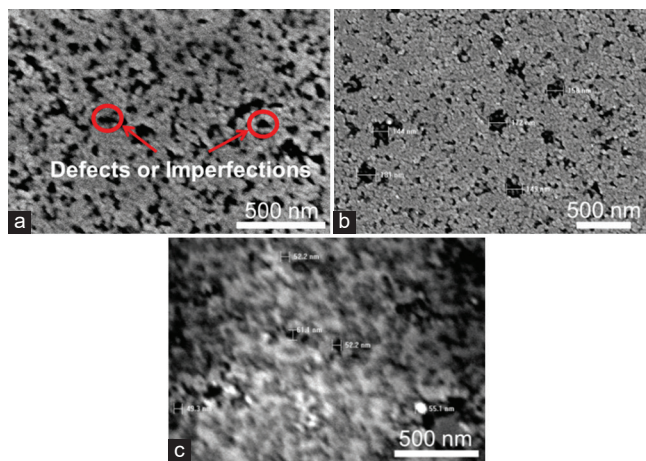


Fig. 5. Examples of high-resolution scanning electron microscopy micrographs showing the surface of nickel film prepared under 40 s deposition time at (a-c) three different locations.

In spite of the surface non-uniformity of these films, which was beyond the limit of the GIXR technique, the structural surface variations were confirmed, as demonstrated in Fig. 6, which shows the true specular and simulated scans of electrodeposited Ni films with deposition times of (a) 40 s and (b) 60 s. The true specular scan was fitted using Bede REFS simulations program (Bede REFS, 2007) which is based on the Parratt recursive formulism (Cullity and Stock, 2001). Using this simulation package, the thickness was found to be ~22, ~31, and ~228 nm for Ni films produced at 30 s, 40 s, and 60 s, respectively. The details of this simulation package and GIXR system can be found elsewhere (Bowen and Tanner, 2006; Bowen and Mendis, 2012; Brundle, Evans and Wilson, 1992; Cullity and Stock, 2001; Jordan Valley, 2007; 2008; Parratt, 1954; Wormington, et al., 1999).

Fig. 7 shows an example of XRD pattern of Ni film fabricated under a 60 s deposition time. As expected (Jin, et al., 2003; Rheem, et al., 2007), the crystalline structure of

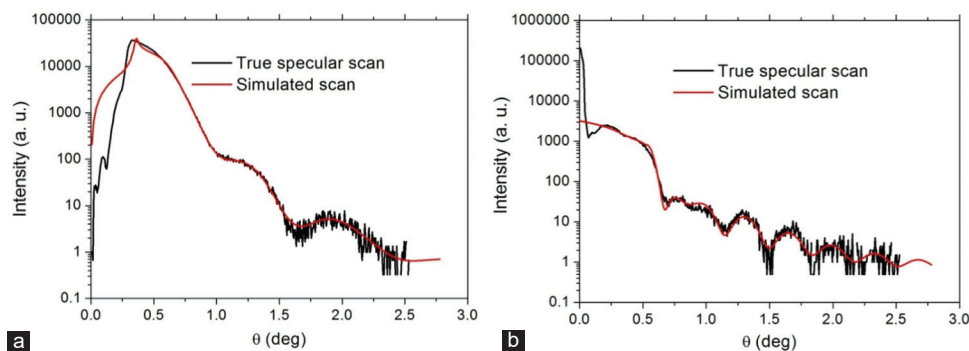


Fig. 6. True specular and simulated scans of electrodeposited nickel films with deposition times of (a) 40 s and (b) 60 s.

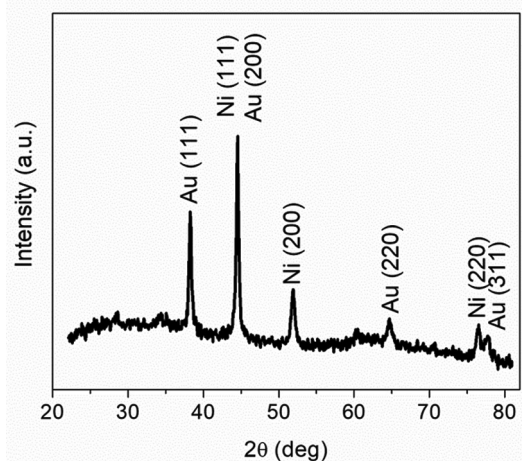


Fig. 7. Example of an X-ray diffraction pattern of the nickel film prepared at 60 s deposition time.

such films is FCC structure, where the peaks correspond to the FCC phase of Ni and the FCC of the Au-coated substrate, as compared with the standard reference patterns (Inorganic Crystal Structure Data base [ICSD]) (Mark, 2023).

From Fig. 7, it is also clear that there are no peaks related to the Si, SiO₂, and Cr elements due to the dominance of the amorphous SiO₂ layer on the behavior, which is in full agreement with the literature (Jian, et al., 2005). Furthermore, the peaks are quite sharp, indicating that the crystallites within such films are relatively large (Bowen and Tanner, 2006; Brundle, Evans and Wilson, 1992; Cullity and Stock, 2001). The intensity of the peaks is related to the presence of a preferred crystallite orientation or the sample thickness. The calculated intensity ratio of the Ni peaks shows that these samples have no preferred orientation in any direction. This result means that there is no effect of crystallites on the magnetization behavior, as will be seen in the following discussion.

B. Moke Measurements – Magnetic Properties

To discuss the distribution of magnetization across the whole sample area and to deeply understand the angular dependence of the magnetic state of such films, MOKE measurements were carried out at different arbitrary places (A, B, C, D, and E shown in Fig. 1a) on these films when the magnetic field was applied at two orthogonal angles with respect to the chip long axis (defined in Fig. 1a).

In general, square hysteresis loops were obtained from most of these studies, with very small local variations. Typical examples of MOKE loops obtained from such measurements are shown in Fig. 8. The similarity in the hysteresis shape among the majority of cases indicated an isotropic magnetic nature in the surface plane of such films. The reversal behavior was sharper for samples with higher growth times and more rounded for samples with lower deposition times.

To understand in more detail the magnetic state in these films, distribution histograms of the coercive field were obtained by repeating the measurements at many different positions on these films, as shown in Fig. 9a. The average coercivity as a function of film growth time is also shown in Fig. 9b. A reduction in coercivity was observed with increased growth time. As an example, the coercivity peaked around ~67 Oe, ~65 Oe, and ~35 Oe for samples with growth times of 30 s, 40 s, and 60 s, respectively. It has also been noticed from Fig. 9 that there is a broad distribution of coercivity throughout the film area of the same sample, which decreases considerably for samples with longer growth times. As an example, the distribution of coercivity was found to range between approximately 24–35 Oe and 58–85 Oe for the samples with the longest (60 s) and shortest (30 s) deposition times, respectively.

The coercivity distributions obtained here may reasonably be attributed to the changes in the film surface morphology discussed earlier in the previous section by HRSEM and GIXR measurements. This result is in full agreement with the result reported in the literature (Oliveira, Rezende, and Azevedo, 2008), which showed that the presence of surface structural variations (defects or imperfections) can act as pinning centers during the reversal, distort the spin configuration structure, and give different values of coercive field (Oliveira, Rezende, and Azevedo, 2008).

Hence, the surface structural variations in the samples under investigation may contribute to the change observed in the coercive field and the shape of the MOKE hysteresis loops. Fig. 9b clearly shows that decreasing the growth time decreases the film thickness, which, in turn, increases the film surface structure variations and non-uniformity and ultimately increases the pinning sites and coercive fields.

To understand the magnetic reversal in such ferromagnetic thin films, the average coercivity as a function of sample

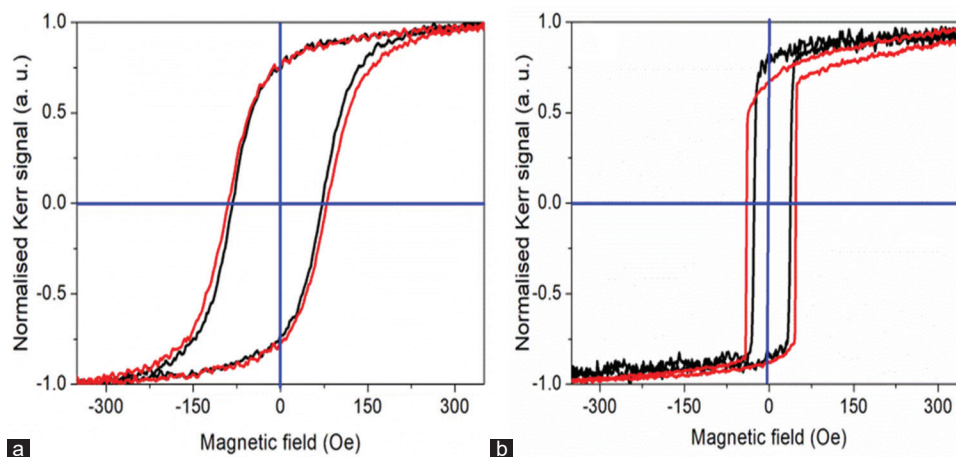


Fig. 8. Normalized Magneto-Optical Kerr Effect hysteresis loops of electrodeposited nickel films prepared under (a) 30 s and (b) 60 s growth times and measured along two perpendicular in-plane axes.

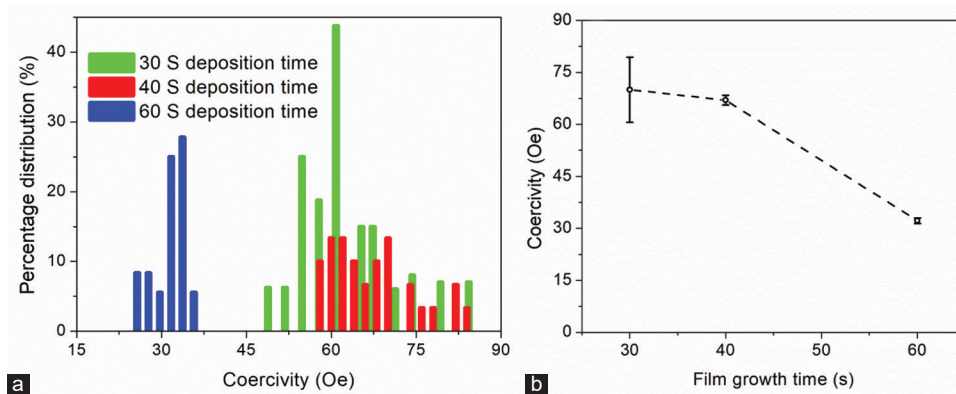


Fig. 9. (a) Distribution histogram of the coercive field acquired from repeating Magneto-Optical Kerr Effect examinations on the electrodeposited nickel films at different arbitrary positions; and (b) average coercive field as a function of deposition time.

long axis angles with respect to the externally applied magnetic field is plotted in Fig. 10. Clearly, for each chip, the coercive field was nearly constant (dash line) for most angles discussed here, indicating the similarity in the magnetization reversal in these samples. The similarity in the reversal behavior, however, might be due to the lack of preferred orientation of the crystallites within such Ni thin films, as confirmed by the XRD measurements stated previously. However, the data for the shortest deposition time (30 s) demonstrate an increase in coercive field with a broader distribution of different angles. This may also reflect the differences in surface morphology discussed earlier. Nonetheless, the results acquired here give an indication that these films are soft at longer growth times and are generally isotropic.

Now, to gain a fuller understanding of the magnetic properties of such films, the coercivity acquired here was compared with other results reported in the literature discussing isolated Ni and NiFe nanowires prepared under the same conditions and measured also by MOKE magnetometry (Sultan, et al., 2012; Sultan, 2017a; 2017b; 2018), a large difference was noticed. This large difference is quite acceptable since the crystallites within such ferromagnetic thin films have no preferred orientations and

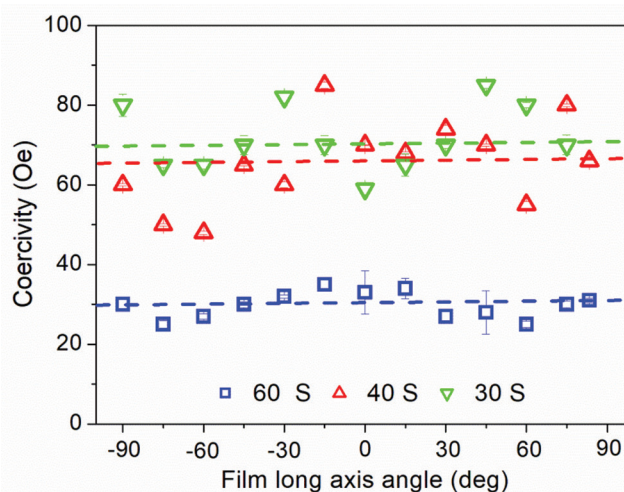


Fig. 10. Derived coercivity from the loops obtained from Magneto-Optical Kerr Effect measurements at various positions on the electrodeposited Ni films (with different deposition times as indicated in the figure title) as a function of the sample long axis angle with respect to the applied magnetic field. The dashed lines provide a guide for the eye.

have no shape anisotropy dominating the behavior as in the nanowires.

C. MR Measurements – Electrical and Magnetic Properties

The electro- and magneto-transport measurements of these films were implemented by applying an external magnetic field in two orthogonal directions with respect to the current flow (sample long axis) using a four-point probe arrangement (Fig. 3) after connecting these samples to the external electrical circuit. The measured electrical resistance, R_o , (overall sample resistance) at zero field for these films with deposition times of 40 s and 60s, was $\sim 26.4 \Omega$ and $\sim 3.4 \Omega$, respectively, and the behavior was ohmic. The electrical resistance of such films is expected to be relatively lower than that of individual nanowires (see, for example, References [Cullity and Graham, 2009; Rheem, et al., 2007]). This is due to the large sizes of the samples investigated here with respect to their counterpart’s ferromagnetic nanowires and the increased volume-to-surface ratio. This resistance, however, is due to the sample bulk resistance, R_s , connected wire resistance, R_w , and contact resistance, R_c .

The value of the sample resistance, R_s , depends on various parameters, such as the dimension of the chip, the scattering rates of the electrons with phonons, defects, and grain boundaries within the films (Rheem, et al., 2007). On the other hand, the connection wire resistance, R_w , appears as a result of the electrical connection of these films with the external electrical circuitry. This electrical resistance is extremely small and can be neglected. Finally, the contact resistance, R_c , arises from the connections of the four probes with the samples. This resistance, however, arises as a result of the presence of hydroxide or oxide layers or any other residual impurities on these chips, as discussed elsewhere. Thus, the overall electrical resistance, R_o , in such films can be written as:

$$R_o = R_s + R_w + R_c \quad (1)$$

The sample resistance, R_s , was estimated approximately depending on the film size and their bulk resistivity ($\rho = \sim 6.99 \times 10^{-8} \Omega \cdot \text{cm}$ at room temperature) using the following relation (Cullity and Graham, 2009; Helmenstine, 2020; Jiles, 1998; Sultan, 2017):

$$R_s = \rho L/A \quad (2)$$

where, L and A are the length and cross-sectional area of the Ni film, respectively. Accordingly, the calculated sample resistance was found to be $\sim 20.3 \Omega$ and $\sim 2.8 \Omega$ for films

with growth times of 40 s and 60 s, respectively. Comparing this theoretical result with the experimental result discussed earlier from MR measurements, an agreement is clearly seen, which is quite reasonable since the rest of the electrical resistances belonged to the contact resistance, R_c , and wire resistance, R_w .

Fig. 11 shows typical results obtained from these MR measurements of Ni films with deposition times of (a) 40 s and (b) 60 s by applying the external magnetic field in longitudinal (parallel) and transverse (normal) orientations to the sample long axis. These experiments were performed 4 times by sweeping the external magnetic field in both directions, as shown in Fig. 11. From these MR measurements, it is interesting to note the excellent quality of the signal-to-noise ratio. For both samples and both longitudinal and transverse profiles, two regions were recognized (Fig. 11). At high magnetic field strengths $\geq \pm 150$ Oe, the resistance shows saturation, indicating that the spins within these films are directed normal (with minimum electrical resistance) and parallel (with maximum electrical resistance) to the applied external magnetic field. At magnetic fields $\leq \pm 150$ Oe, the resistance falls rapidly, followed by positive jumps in the parallel directions, and jumps up, followed by a drop in the orthogonal directions. The variations in electrical resistance are symmetric about the zero magnetic fields when changing the magnetic field direction.

Comparing the electrical resistance of longitudinal and transverse measurements with each other at maximum field strengths (saturation), a reduction in the saturated resistance was seen as the implementation changed from parallel to perpendicular directions. This can be understood in terms of the magnetic spin orientations within these films. When the spins lie parallel (normal) to the film’s long axis, the magnetization will be collinear (orthogonal) to the current flow, giving maximum (minimum) electrical resistance. This is the maximum and minimum electrical resistance relative to the current and magnetic moments in the AMR effect (Cullity and Graham, 2009; Armstrong, 2010; Jian, et al., 2005).

The difference in resistance, δR , is defined as the changes between the resistance when the external applied magnetic field is longitudinal, R_L , and transverse, R_T , to the current flow (demonstrated in Fig. 11b), and it is given by (Brundle, Evans and Wilson, 1992; Sultan, 2013):

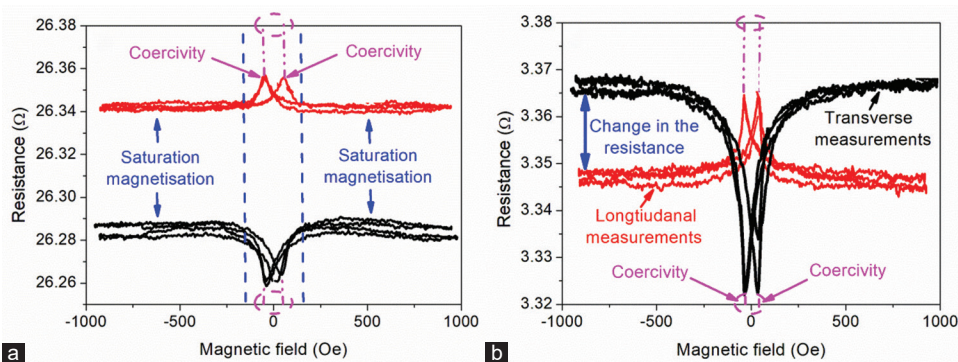


Fig. 11. Magneto-resistance profiles obtained from electrodeposited nickel samples with (a) 40 s and (b) 60 s deposition times by applying the external magnetic field either longitudinally (parallel) or transversely (perpendicular) to the current flow.

$$\delta R = R_{\parallel} - R_{\perp} \quad (3)$$

The difference in resistance, δR , for the sample with a 40 s deposition time was found to be 0.06 Ω , which is larger than the difference in resistance (0.02 Ω) of the films with a 60 s deposition time.

Since the electrical resistance in the absence of the external magnetic field depends on the structure of the domain, which depends on the magnetic history of the sample, it is more suitable to use the following equation to show the average electrical resistance (Armstrong, 2010):

$$R_{ave} = \frac{1}{3}(R_{\parallel} + 2R_{\perp}) \quad (4)$$

The δR of a ferromagnetic sample on applying an external magnetic field is usually expressed as $\delta R/R_{ave}$, and is known as the AMR ratio, which is given by combining equations 3 and 4 (Yoo, et al., 2006):

$$\frac{\delta R}{R_{ave}} = \frac{R_{\parallel} - R_{\perp}}{\frac{1}{3}(R_{\parallel} + 2R_{\perp})} \quad (5)$$

Thus, the AMR ratio was calculated here using equation 5, and it was found to be ~ 0.7 and ~ 1.8 for samples with 40 s and 60 s growth times, respectively. The difference between these values can be attributed to the difference in film thickness. Comparing the AMR ratio obtained here with the AMR ratio reported in the literature for individual nanowires with the same composition and prepared under similar conditions, an agreement was noticed (Yoo, et al., 2006).

As discussed earlier, the average coercive field acquired from MOKE hysteresis loops of Ni films of 40 s and 60 s deposition times (Fig. 9) was ~ 67 Oe and ~ 35 Oe, respectively. Comparing these findings with the coercivities extracted from the magnetic fields at which the peaks (troughs) happened in the MR profiles (Fig. 11), an excellent agreement was found, indicating that the magnetic state at the surface of such films behaves similarly to that of their bulks. This result is quite reasonable since the thickness of these films is extremely thin. Finally, studying the saturation magnetization and annealing the samples under different temperatures (Kamrul and Johurul, 2015) are very important and needs further research.

IV. CONCLUSIONS

To sum up, the magnetic and electrical properties of electrodeposited Ni thin films prepared at different growth times were studied in detail. The chemical composition of these films was analyzed using EDS measurements, which confirm that these films are free from impurities and contamination. HRSEM measurements indicated the existence of defects or imperfections distributed randomly on these samples. These imperfections were attributed to the inhomogeneous density of the electrolyte solution throughout the electrochemical cell or to the occurrence of gas bubbles during the fabrication process. Thus, the Ni films prepared using this technique under such conditions is more likely to be non-uniform and have an irregular surface morphology. XRD analysis showed that

the crystalline structure of such films is FCC with quite large crystallites of no preferred orientation in any direction.

MOKE measurements were executed at many arbitrary locations on these films by applying the magnetic field at different angles with respect to the sample's long axis. Square loops were noticed with a high squareness ratio. The similarity in the hysteresis shape between the two orthogonal in-plane axes in most measurements indicates an isotropic magnetic nature in such films. This result was attributed to the lack of preferred orientation of the crystallites within such samples, as confirmed by XRD measurements. The coercivity falls by increasing the film growth time (~ 67 Oe to ~ 35 Oe for samples with growth times of 30–60 s, respectively). This was attributed to a reduction in surface non-uniformity on increasing the film thickness, which, in turn, minimizes the pinning sites and coercive fields. The experimental and theoretical resistances were in agreement with each other and were found to be around 20.3 Ω and 2.8 Ω for films with growth times of 40 s and 60 s, respectively. The difference in resistance, δR , for the sample with a 40 s deposition time was found to be ~ 0.06 Ω , which is larger than the difference in resistance ~ 0.02 Ω of the films with a 60 s deposition time. This result was in full agreement with the literature. The coercivities acquired from MR measurements were consistent with the coercivities obtained from MOKE measurements, indicating that the magnetization at the surface of such films behaves similarly to that of their bulks.

ACKNOWLEDGMENTS

The author wishes to express his deep sense of appreciation and many thanks to Prof. Dr. Del Atkinson at the Physics Department, Durham University, England, for his valuable assistance throughout this work. Acknowledgments are also due to Dr. Jennifer King, Dr. Bipul Das, and Prof. Dr. Kalyan Mandal for providing these Ni samples.

REFERENCES

- Alcer, D., and Atkinson, D., 2017. The role of mesoscopic structuring on the intermixing of spin-polarised conduction channels in thin-film ferromagnets for spintronics. *Nanotechnology*, 28(37), p.375703.
- Allwood, D.A., Xiong, G., Cooke, M.D., and Cowburn, R.P., 2003. Magneto-optical Kerr effect analysis of magnetic nanostructures. *Journal of Physics D: Applied Physics*, 36, p.2175.
- Allwood, D.A., Xiong, G., Faulkner, C.C., Atkinson, D., Petit, D., and Cowburn, R.P., 2005. Magnetic domain-wall logic. *Science*, 309, p.1688.
- Aravamudhan, S., Singleton, J., Goddard, P.A., and Bhansali, S., 2009. Magnetic properties of Ni-Fe nanowire arrays: Effect of template material and deposition conditions. *Journal of Physics D: Applied Physics*, 42, p.115008.
- Armstrong, H., 2010. *Magnetoresistance Measurement System Instruction Manual V3.0*. Durham University, Physics Department, Durham, England [Last accessed on 2023 Nov 28].
- Atkinson, D., Eastwood, D.S., and Bogart, L.K., 2008. Controlling domain wall pinning in planar nanowires by selecting domain wall type and its application in a memory concept. *Applied Physics Letters*, 92(2), p.022510.
- Azzawi, S., Ganguly, A., Tokaç, M., Rowan-Robinson, R.M., Sinha, J., Hindmarch, A.T., Barman, A., and Atkinson, D., 2016. Evolution of damping

- in ferromagnetic/nonmagnetic thin film bilayers as a function of nonmagnetic layer thickness. *Physical Review B*, 93(5), p.054402.
- Bede REFS., 2007. (*Version 4.5*): *User Manual, Bede PLC, Durham*. Available from: <https://jordanvalleyplc> [Last accessed on 2023 Nov 28].
- Bowen, K.D., and Tanner, B.K., 2006. *X-Ray Metrology in Semiconductor Manufacturing*. Taylor and Francis Group, LLC, United Kingdom.
- Bowen, L., and Mendis, B., 2012. *Electron Microscopy Facility. Physics Department, Durham University, U.K.*, in Private Communication.
- Brundle, R.C., Evans, C.A. Jr., and Wilson, S., 1992. *Encyclopaedia of Materials Characterization*. Butterworth-Heinemann, a division of Reed publishing Inc., Oxford.
- Bryan, M.T., Atkinson, D., and Allwood, D.A., 2006. Multimode switching induced by a transverse field in planar magnetic nanowires *Applied Physics Letters*, 88(3), p.032505.
- Chen, T.C., Kuo, C.Y., Mishra, A.K., Das, B., and Wu, J.C., 2015. Magnetic domain wall motion in notch patterned permalloy nanowire devices. *Physica B: Condensed Matter*, 476, p.161.
- Coe, J.M.D., and Hinds, G., 2001. Magnetic electrodeposition. *Journal of Alloys and Compounds*, 326(1-2), pp.238-245.
- Cullity, B.D., and Graham, C.D., 2009. *Introduction to Magnetic Materials*. 2nd ed., John Wiley and Sons Inc., Hoboken, New Jersey.
- Cullity, B.D., and Stock, S.R., 2001. *Elements of X-Ray Diffraction*. 3rd ed., Prentice-Hall Inc., Hoboken.
- Daimon, H., and Kitakami, O., 1993. Magnetic and crystallographic study of Co electrodeposited alumite films. *Journal of Applied Physics*, 73(10), p.5391.
- Das, B., Chen, T.C., Shiu, D.S., Lance, H., and Wu, J.C., 2016. Differential domain wall propagation in Y-shaped permalloy nanowire devices. *World Science*, 6(1), p.1650006.
- Das, B., Mandal, K., Sen, P., and Bandopadhyay, S.K., 2008. Effect of aspect ratio on the magnetic properties of nickel nanowires. *Journal of Applied Physics*, 103, p.013908.
- Donald, M.M., 2003. *The Foundations of Vacuum Coating Technology*. Noyes Publications William Andrew Publishing Norwich, New York.
- Eastwood, D., 2009. *Technical Note DSE4, Durham Longitudinal Focused MOKE: Operation Guide*. Physics Department, Durham University, UK.
- Eider, B., Cristina, B., Miriam, J., Manuel, V., and Agustina, A., 2016. Domain wall pinning in FeCoCu bamboo-like nanowires. *Scientific Reports*, 6, p.29702.
- Elhoussine, F., Vila, L., Piraux, L., and Faini, G., 2005. Multiprobe perpendicular giant magnetoresistance measurements on isolated multilayered nanowires. *Journal of Magnetism and Magnetic Materials*, 290-291, pp.116-119.
- Ester, M.P., Cristina, B., del Real, R.P., and Manuel, V., 2015. Vortex domain wall propagation in periodically modulated diameter FeCoCu nanowire as determined by the magneto-optical Kerr effect. *Nanotechnology*, 26, p.461001.
- Fernández-Pacheco, A., De Teresa, J.M., Córdoba, R., and Ibarra, M.R., 2008. Magnetotransport properties of high-quality cobalt nanowires grown by focused-electron-beam-induced deposition. *Journal of Physics D: Applied Physics*, 42, p.055005.
- Fernández-Pacheco, A., De Teresa, J.M., Szkudlarek, A., Córdoba, R., Ibarra, M.R., Petit, D., O'Brien, L., Zeng, H.T., Lewis, E.R., Read, D.E., and Cowburn, R.P., 2009. Magnetization reversal in individual cobalt micro- and nanowires grown by focused-electron-beam-induced-deposition. *Nanotechnology*, 20(47), p.475704.
- Ferré, R., Ounadjela, K., George, J.M., Piraux, L., and Dubois, S., 1997. Magnetization processes in nickel and cobalt electrodeposited nanowires. *Physical Review B*, 56(21), pp.14066-14075.
- Fert, A., and Piraux, L., 1999. Magnetic nanowires. *Journal of Magnetism and Magnetic Materials*, 200, pp.338-358.
- Ganguly, A., Azzawi, S., Saha, S., King, J.A., Rowan-Robinson, R.M., Hindmarch, A.T., Sinha, J., Atkinson, D., and Barman, A., 2015. Tunable magnetization dynamics in interfacially modified Ni₈₁Fe₁₉/Pt bilayer thin film microstructures. *Scientific Reports*, 5, p.17596.
- Guo, Y., Qin, D.H., Ding, J.B., and Li, H.L., 2003. Annealing and morphology effects on the Fe_{0.39}Co_{0.61} nanowire arrays. *Applied Surface Science*, 218(1-4), pp.107-113.
- Helmenstine, A.M., 2020. *Table of Electrical Resistivity and Conductivity*. ThoughtCo, New York. Available from: <https://thoughtco.com/table-of-electrical-resistivity-conductivity-608499> [Last accessed on 2023 Nov 28].
- Heyderman, L.J., Solak, H.H., David, C., Atkinson, D., Cowburn, R.P., and Nolting, F., 2004. Arrays of nanoscale magnetic dots: Fabrication by x-ray interference lithography and characterization. *Applied Physics Letters*, 85(21), p.4989.
- Jian, Q., Josep, N., Maria, M., Anna, R., Juan, S.M., and Mamoun, M., 2005. Differences in the magnetic properties of Co, Fe, and Ni 250-300 nm wide nanowires electrodeposited in amorphous anodized alumina templates. *Chemistry of Materials*, 17, pp.1829-1834.
- Jiles, D., 1998. *Introduction to Magnetism and Magnetic Materials*. 2nd ed., Chapman and Hall/CRC, New York.
- Jin, C.G., Liu, W.F., Jia, C., Xiang, X.Q., Cai, W.L., Yao, L.Z., and Li, X.G., 2003. High-filling, large-area Ni nanowire arrays and the magnetic properties. *Journal of Crystal Growth*, 258, pp.337-341.
- Jordan Valley applications Staff., 2007. In: Lafford, T., Ryan, P., Wormington, M., Matney, K., Jacques, D., Bytheway, R., Bo, Q., Hofmann, F., and Trussell, R. (eds). *Bede X-Ray Applications Manual*. Jordan Valley Semiconductors Ltd., Texas.
- Jordan Valley applications staff., 2008. Lafford, T., Ryan, P., Wormington, M., Matney, K., Jacques, D., Bytheway, R., Bo, Q., Hofmann, F., and Trussell, R. (eds). *D1 Installation, Operation and Maintains Manual*. Jordan Valley Semiconductors Ltd., Texas.
- Kacel, T., Guittoum, A., Hemmous, M., Dirican, E., Öksüzoglu, R.M., Azizi, A., Laggoun, A., and Zergoug, M., 2018. Effect of thickness on the structural, microstructural, electrical and magnetic properties of Ni films elaborated by pulsed electrodeposition on Si substrate. *Surface Review and Letters*, 25(2), p.1850058.
- Kafil, M.R., Fernando, M.F.R., and Saibal, R., 2009. Magnetic properties of nickel nanowires: Effect of deposition temperature. *Journal of Applied Physics*, 105, p.083922.
- Kamrul, H.M., and Johurul, I.M., 2015. Effect of Substrate and Annealing on Electrical, Magnetic and Morphological Properties of Ni Thin Films. In: *International Conference on Materials, Electronics and Information Engineering, ICMEIE*.
- Karahan, I.H., Bakkalo, O.F., and Bedir, M., 2007. Giant magnetoresistance of electrodeposited Cu-Co-Ni alloy film. *Pramana-Journal of Physics*, 68, pp.83-90.
- Koohbor, M., Soltanian, S., Najafi, M., and Servati, P., 2012. Fabrication of CoZn alloy nanowire arrays: Significant improvement in magnetic properties by annealing process. *Materials Chemistry and Physics*, 131(3), pp.728-734.
- Kunz, A., Reiff, S.C., Priem, J.D., and Rentsch, E.W., 2010. Controlling Individual Domain Walls in Ferromagnetic Nanowires for Memory and Sensor Applications. In: *International Conference on Electromagnetics in Advanced Applications*, p.248.
- Lee, S.W., Jeong, M.C., Myoung, J.M., Chae, G.S., and Chung, I.J., 2007. Magnetic alignment of ZnO nanowires for optoelectronic device applications. *Applied Physics Letters*, 90(13), p.133115.
- Lihu, L., Haitao, L., Shenghua, F., Jianjun, G., Yaopeng, L., and Huiyuan, S., 2009. Fabrication and magnetic properties of Ni-Zn nanowire arrays. *Journal of Magnetism and Magnetic Materials*, 321, pp.3511-3514.
- Lodder, J.C., 2004. Methods for preparing patterned media for high-density recording. *Journal of Magnetism and Magnetic Materials*, 272-276.

pp.1692-1697.

Lupu, N., Lostun, M., and Chiriac, H., 2010. Surface magnetization processes in soft magnetic nanowires. *Journal of Applied Physics*, 107(9), p.09E315.

Mark, W., 1993-2023. *Web Elements*. Available from: <https://www.webelements.com> [Last accessed on 2023 Nov 28].

Maruyama, K., Namikawa, K., Konno, M., and Maruyama, H., 1997. Magnetization process of iron surface observed by transverse Kerr magnetometry. *Journal of Applied Physics*, 81(8), pp.5675-5677.

Michelini, F., Ressler, L., Degauque, J., Baule's, P., Fert, A.R., Peyrade, J.P., and Bobo, J.F., 2002. Permalloy thin films on MgO (001): Epitaxial growth and physical properties. *Journal of Applied Physics*, 92, pp. 7337-7340.

Murakami, M., and Birukawa, M., 2008. Sputtering gases and pressure effects on the microstructure, magnetic properties and recording performance of TbFeCo films. *Journal of Magnetism and Magnetic Materials*, 320(5), pp.608-611.

Nasirpour, F., 2007. Template electrodeposition of magnetic nanowire arrays. *Transworld Research Network*, 661, p.37.

Nazila, D., and Georges, J.K., 2007. Electroless fabrication of cobalt alloys nanowires within alumina template. *Journal of Nanomaterials*, 2007, p.46919.

Oliveira, A.B., de Silva, G.L., Rezende, S.M., and Azevedo, A., 2010. Magnetization reversal in single ferromagnetic rectangular nanowires. *Journal of Physics: Conference Series*, 200(7), p.072023.

Oliveira, A.B., Rezende, S.M., and Azevedo, A., 2008. Magnetization reversal in permalloy ferromagnetic nanowires investigated with magnetoresistance measurements. *Physical Review B*, 78(2), p.024423.

Parlaka, U., Aköz, M.E., Tokdemir Öztürk, S., and Erkovanc, M., 2015. Thickness dependent magnetic properties of polycrystalline nickel thin films. *Acta Physica Polonica Series A*, 127(4), pp.995-997.

Parratt, G.L., 1954. Surface studies of solids by total reflection of X-rays. *Physical Review*, 95, p.359.

Peter, T.T., 2008. *Utilising Electrochemical Deposition for Micro Manufacturing*. Cardiff University, Whittles Publishing Ltd., Cardiff, UK.

Philip, S., Javier, G.F., Stefan, M., Michael, Z., Tim, B., Victor, V.M., de la Prida, V.M., Detlef, G., and Kornelius, N., 2016. Statistical magnetometry on isolated NiCo nanowires and nanowire arrays: A comparative study. *Journal of Physics D: Applied Physics*, 49(14), p.145005.

Pignard, S., Goglio, G., Radulescu, A., Piroux, L., Dubois, S., Declémy, A., and Duval, J.L., 2000. Study of the magnetization reversal in individual nickel nanowires. *Journal of Applied Physics*, 87(2), pp.824-829.

Possin, E.G., 1970. A method for forming very small diameter wires. *Review of Scientific Instruments*, 41, pp.772-774.

Qin, D.H., Wang, C.W., Sun, Q.Y., and Li, H.L., 2002. The effects of annealing on the structure and magnetic properties of CoNi patterned nanowire arrays. *Applied Physics A*, 74, pp.761-765.

Rahman, I.Z., Razeed, K.M., Kamruzzaman, M., and Serantoni, M., 2004. Characterisation of electrodeposited nickel nanowires using NCA template. *Journal of Materials Processing Technology*, 153-154, pp.811-815.

Ren, Y., Liu, Q.F., Li, S.L., Wang, J.B., and Han, X.H., 2009. The effect of structure on magnetic properties of Co nanowire arrays. *Journal of Magnetism and Magnetic Materials*, 321(3), pp.226-230.

Rheem, Y., Yoo, B.Y., Beyermann, W.P., and Myung, N.V., 2007a. Magnetotransport studies of a single nickel nanowire. *Nanotechnology*, 18, p.015202.

Rheem, Y., Yoo, B.Y., Beyermann, W.P., and Myung, N.V., 2007c. Magneto-transport studies of single ferromagnetic nanowire. *Physica Status Solidi (A)*, 204(12), pp.4004-4008.

Rheem, Y., Yoo, B.Y., Beyermann, W.P., and Myung, N.V., 2007d. Electro-and

magneto-transport properties of a single CoNi nanowire. *Nanotechnology*, 18(12), p.125204.

Rheem, Y., Yoo, B.Y., Koo, B.K., Beyermann, W.P., and Myung, N.V., 2007b. Synthesis and magnetotransport studies of single nickel-rich NiFe nanowire. *Journal of Physics D: Applied Physics*, 40(23), p.7267.

Rizwan, M.N., Bell, C., Kalyar, M.A., Makhdoom, A.R., Anwar-ul-Haq, M., and Gilory M., 2021. Structural, magnetic and electrical properties of nickel thin films deposited on Si (100) substrates by pulsed laser deposition. *Journal of Ovonic Research*, 17(3), pp.225-230.

Sharma, S., Barman, A., Sharma, M., Shelford, L.R., Kruglyak, V.V., and Hicken, R.J., 2009. Structural and magnetic properties of electrodeposited cobalt nanowire arrays. *Solid State Communications*, 149(39), pp.1650-1653.

Sultan, M.S., 2013. *Experimental and Micromagnetic Study of Magnetisation Behaviour in Isolated Ferromagnetic Nanowires*. PhD thesis submitted to Durham University.

Sultan, M.S., 2017a. Angular dependence of switching behaviour in template released isolated NiFe nanowires. *Physics Letters A*, 381(46), pp.3896-3903.

Sultan, M.S., 2017b. Surface morphology and magnetic properties of isolated cylindrical nickel nanowires. *American Journal of Nanosciences*, 3(3), pp.30-38.

Sultan, M.S., 2017c. Electro- and magneto-transport behavior of template-released isolated ferromagnetic nanowires. *IEEE Transactions on Magnetics*, 53(12), pp.1-10.

Sultan, M.S., 2018. Magnetic State of Template Released Isolated Nickel Nanowires. In: *International Conference on Pure and Applied Science*, Koya University, Kurdistan.

Sultan, M.S., Das, B., Sen, P., Mandal, K., and Atkinson, D., 2012. Template released ferromagnetic nanowires: Morphology and magnetic properties. *Journal of Spintronics and Magnetic Nanomaterials*, 1(1), pp.113-121.

Sun, L., and Chen, Q., 2009. Magnetic field effects on the formation and properties of nickel nanostructures. *European Journal of Inorganic Chemistry*, 2009, pp.435-440.

Sun, L., Hao, Y., Chien, C.L., and Searson, P.C., 2005. Tuning the properties of magnetic nanowires. *IBM Journal of Research and Development*, 49(1), pp.79-102.

Thompson, S.M., 2008. The discovery, development and future of GMR: The nobel prize 2007. *Journal of Physics D: Applied Physics*, 41, p.093001.

Tian, F., Chen, J., Zhu, J., and Wei, D., 2008. Magnetism of thin polycrystalline nickel nanowires. *Journal of Applied Physics*, 103, p.013901.

Tian, F., Zhu, J., Wei, D., and Shen, Y.T., 2005. Magnetic field assisting DC electrodeposition: General methods for high-performance Ni nanowire array fabrication. *The Journal of Physical Chemistry B*, 109, p.14852.

Tokaç, M., Wang, M., Jaiswal, S., Rushforth, A.W., Gallagher, B.L., Atkinson, D., and Hindmarch, A.T., 2015. Interfacial contribution to thickness dependent in-plane anisotropic magnetoresistance. *AIP Advances*, 5(12), p.127108.

Uehara, Y., and Ikeda, S., 2003. Dependence of magnetic properties on sputtering pressure for Fe-Al-O alloy films made by carousel-type sputtering. *Japanese Journal of Applied Physics*, 42(7A), pp.4297-4301.

Vega, V., Bohnert, T., Martens, S., Waleczek, M., Montero-Moreno, J.M., Görlitz, D., Prida, V.M., and Nielsch, K., 2012. Tuning the magnetic anisotropy of Co-Ni nanowires: Comparison between single nanowires and nanowire arrays in hard-anodic aluminum oxide membranes. *Nanotechnology*, 23(46), p.465709.

Wormington, M., Panaccione, C., Matney, K.M., and Bowen, D.K., 1999. Characterization of structures from X-ray scattering data using genetic algorithms. *Philosophical Transactions of the Royal Society of London-Series A*, 357, pp.2827-2848.

Yoo, B., Rheem, Y., Beyermann, W.P., and Myung, N.V., 2006. Magnetically assembled 30 nm diameter nickel nanowire with ferromagnetic electrodes. *Nanotechnology*, 17(10), pp.2512-2517.